Available online at www.sciencedirect.com
ScienceDirect
Trans. Nonferrous Met. Soc. China 32(2022) 3534−3549
Transactions of Nonferrous Metals Society of China
www.tnmsc.cn

Role of yttrium content in twinning behavior of extruded Mg−Y sheets under tension/compression

Yan-qin CHAI[1], Dong-di YIN[1], Shen HUA[1], Guang-hao HUANG[1], Hao ZHOU[2], Jiang ZHENG[3], Qu-dong WANG[4]

1. Key Laboratory of Advanced Technologies of Materials, Ministry of Education, School of Materials Science and Engineering, Southwest Jiaotong University, Chengdu 610031, China;
2. Nano and Heterogeneous Materials Center, School of Materials Science and Engineering, Nanjing University of Science and Technology, Nanjing 210094, China;
3. Shenyang National Laboratory for Materials Science, International Joint Laboratory for Light Alloys (Ministry of Education), College of Materials Science and Engineering, Chongqing University, Chongqing 400044, China;
4. National Engineering Research Center of Light Alloys Net Forming, School of Materials Science and Engineering, Shanghai Jiao Tong University, Shanghai 200240, China

Received 15 September 2021; accepted 5 April 2022

Abstract: The influence of Y content on the grain-scale twinning behavior in extruded Mg−xY (x=0.5, 1, 5, wt.%) sheets under uniaxial tension and compression along the extruded direction was statistically investigated. An automatic twin variant analysis was employed, based on large data sets obtained by electron backscatter diffraction (EBSD), including 2691 grains with 977 twins. The $\{10\bar{1}2\}$ tension twinning (TTW) dominance and prevailing anomalous twinning behavior (Schmid factor (m) <0) under both tension and compression were found. The anomalous twinning behavior was more pronounced as Y content increased under tensile loading, indicating a promoted stochasticity of twin variant selection for more concentrated Mg−Y alloys. However, the trend for the Y-content dependent anomalous twinning behavior was opposite in compression. The fractions of the anomalous TTWs were found to be well correlated with the maximum Schmid factor (m_{max}) values of basal slip and prismatic slip in the corresponding parent grains for compression and tension, respectively, indicating that twinning and dislocation slip might be closely related in the present Mg−Y alloys.

Key words: Mg−RE alloys; deformation twinning; twin variant selection; Schmid factor; anomalous twin

1 Introduction

Magnesium (Mg) alloys have recently drawn extensive attention in lightweight applications due to the characteristics of low density and high specific strength [1−4]. As an alternative deformation mode besides slip, deformation twinning can produce strain in parallel with the c-axis of the crystal lattice and is especially required for coordinating the deformation of hexagonal closed-packed structure (HCP) Mg alloys [5−7]. The poler nature that twinning possesses makes it exhibit more complicated deformation characteristics than slip [8]. Twinning can greatly affect the mechanical response [9,10], strength and ductility [11,12], texture evolution [13,14], and fracture behavior [15,16] of Mg alloys. Therefore, it is significant to study twinning behavior for understanding the deformation mechanism of Mg alloys and controlling their properties.

Corresponding author: Dong-di YIN, Tel: +86-28-87634673, E-mail: ahnydd@swjtu.edu.cn
DOI: 10.1016/S1003-6326(22)66037-0

Of all twinning modes in Mg alloys, $\{10\bar{1}2\}$ tension twinning (TTW) is the most common one owing to the low critical resolved shear stress (CRSS) and can be easily activated under either tension parallel to the *c*-axis or compression perpendicular to the *c*-axis of the lattice [17,18]. Generous researches have been devoted to promoting a better understanding of twinning behaviors of HCP Mg alloys and their twin variant selection [19,20]. Nevertheless, up to now, some important issues are remained to be clarified.

One of the widely discussed and controversial issues is whether the Schmid law can effectively predict the process of twin variant selection. The Schmid factor (*m*) has long been considered as an effective parameter for twin formation prediction in Mg alloys, and it holds that the higher the *m* is, the easier the twin activation is. However, it has been also found recently that the TTW variants with low even negative *m* values can be active rather than the expected high-*m* twin variants, i.e. the twin variant selection exhibited non-Schmid behavior [21−23]. For example, CHAI et al [23] performed tension loading along the extrusion direction (ED) on an extruded Mg sheet with strong basal texture and observed significant anomalous twinning behavior. All twins observed were TTWs and 57% of them exhibited negative *m* values. Similar results have also been reported by WANG et al [24], who performed in situ *c*-axis compression tests on textured pure Mg and Mg−3Dy/Er alloys by electron backscatter diffraction (EBSD) and electron channeling contrast imaging (ECCI). However, it should be noted that most of the above studies were based on only a few twins and were not statistically significant. In fact, based on the significant heterogeneity of deformation twinning (the occurrence, special distribution, number, morphology, and especially the variant selection of twins exhibiting significant statistical variation over the microstructure) [19,20], KUMAR and BEYERLEIN [20] recently proposed that the deformation twinning (TTW) may exhibit stochastic nature in HCP polycrystals (Mg, Zr, Ti). Thus, it is essential to adopt a statistical perspective in the studies of deformation twinning.

In addition, it has been reported that alloying can greatly influence twinning behaviors. For instance, plenty of research showed that the addition of Al/Zn elements promotes twin nucleation and inhibits its further growth in AZ Mg alloys [25,26]. However, there is a lack of experimental research on the impact of alloying elements on the twin variant selection, especially based on statistical analysis. On the other hand, since adding rare earth elements (Y, Gd, etc.) is an important alloying method for Mg alloys which can impose a notable impact on the ductility and strength of Mg alloys [27,28], it is instructive to statistically study the influence of rare earth elements on the twinning behavior, especially on the variant selection. Our previous study [29] on a series of Mg−Y sheets with different Y contents indicated that the twinning activity was suppressed by increasing Y content, and almost only TTWs were generated no matter under tension or compression loading. Yet, a further detailed twin variant analysis and the role of rare earth Y element concentration playing in the selection of twin variants are still needed to be shed light on.

In this study, a detailed twinning behavior and variant analysis of Mg−*x*Y (*x*=0.5, 1, 5, wt.%) extruded sheets with weakened basal texture after room temperature (RT) monotonic tensile and compressive deformation were performed based on EBSD from a statistical point of view using an automatic twin variant analysis. The impact of Y content together with loading condition on the twin variant selection in Mg−Y alloys was statistically investigated. In addition, the correlation between the anomalous TTWs with $m<0$ and the maximum Schmid factor of dislocation slip for the corresponding parent grain was analyzed.

2 Experimental

The materials employed in the current research were Mg−0.5Y, Mg−1Y, and Mg−5Y (unless otherwise specified, all components in this work are in mass fraction) binary alloys and the actual compositions were Mg−0.3Y, Mg−0.9Y and Mg−4.8Y, respectively. The alloys were all obtained by steel mold casting followed by homogenization and 573 K (300 °C) hot extrusion into sheets with a cross-sectional size of 80 mm in width and 5 mm in thickness.

Flat dog-bone-shaped tension samples and cuboid compression samples were machined from the extruded sheets using electrical discharge machining. The gage dimensions of tensile samples were 18 mm in length, 3 mm in width and 2 mm in thickness, and the dimensions for compression samples were 7.5 mm in length, 5 mm in width and 5 mm in thickness. Note that the length and width of the specimens were parallel to the extrusion direction (ED) and transverse direction (TD), respectively. The uniaxial tension and compression tests were carried out on a universal testing machine (MTS−CMT5105) along the ED until failure, with the initial strain rate of 10^{-3} s^{-1}. For the sake of repeatability and accuracy, no less than three parallel experiments were conducted for each condition. To avoid the machine compliance problems [30], here we took away the sample−machine combined elastic strain from the total strain to obtain the plastic strain.

The crystallographic orientation map of the ED−TD plane was obtained by a JEOL JSM−7800F field emission scanning electron microscope (SEM) equipped with an Oxford Instrument Nordlys Nano EBSD detector. The tensile and compressive specimens were carefully prepared by standard mechanical polishing followed by chemical polishing for 2 s using a solution consisting of ethanol, hydrochloric acid, and nitric acid with a volume ratio of 50:17:6, and then etching for 2 s using a solution containing nitric acid and distilled water with a volume ratio of 1:6 for EBSD characterization, and the step size employed was 0.3−0.8 μm. Note that the sampling positions were near the fracture surfaces. The raw EBSD orientation twinning analysis was conducted automatically using a homemade MATLAB code based on the open-source toolbox MTEX [31,32]. The details of material preparation, mechanical testing and characterization can refer to our previous work [27,28,33,34].

The twin mode and variant analysis procedure are illustrated in Fig. 1, by taking the grain labeled 181-P containing two twins in the Mg−5Y compressive specimen as an example. First, the twinning modes activated were analyzed by EBSD boundary misorientation analysis. Five common twinning modes were considered and their corresponding misorientation angles/axes were as follows [30,35]: 86° $\langle 1\bar{2}10\rangle$ for $\{10\bar{1}2\}$ TTW; 56° $\langle 1\bar{2}10\rangle$ for $\{10\bar{1}1\}$ CTW; 64° $\langle 1\bar{2}10\rangle$ for $\{10\bar{1}3\}$ CTW; 38° $\langle 1\bar{2}10\rangle$ for $\{10\bar{1}1\}-\{10\bar{1}2\}$ DTW; 22° $\langle 1\bar{2}10\rangle$ for $\{10\bar{1}3\}-\{10\bar{1}2\}$ DTW. Both twins in grain 181-P were identified as TTW. Second, the six possible TTW variants' orientations were obtained using the measured patent mean grain orientation by 180° rotation around the twinning direction η_1 [8,36], as defined in Table 1 and visualized in Fig. 1(c). Finally, the orientations of the measured twins were matched with the above-mentioned theoretically calculated six variants and the activated variant was determined based on the smallest misorientation. More information about the twin variant identification can be found in our previous work [23]. Two twins labeled as 148-V1 and 154-V1 in parent grain 181-P were identified as variant 1 (V1) with m=0.23.

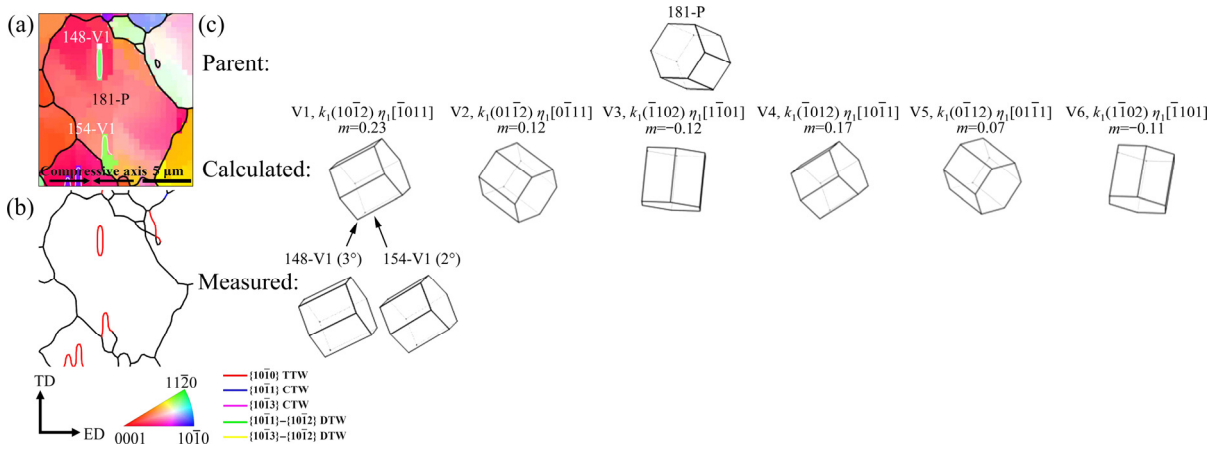

Fig. 1 Illustration of twin variant analysis procedure by taking grain labeled 181-P as an example: (a) IPF map along ND; (b) Twin boundary map; (c) Visualized grain orientation of 181-P, six calculated TTW varients and measured twins

Table 1 Codes, crystallographic indices of six TTW variants and illustration of their twin−parent crystallographic orientation relationship

Twin variant	Twinning system	Schematic diagram
V1	$(10\bar{1}2)[\bar{1}011]$	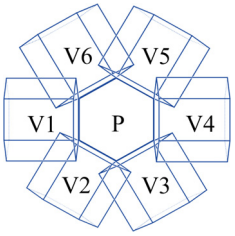
V2	$(01\bar{1}2)[0\bar{1}11]$	
V3	$(\bar{1}102)[1\bar{1}01]$	
V4	$(\bar{1}012)[10\bar{1}1]$	
V5	$(0\bar{1}12)[01\bar{1}1]$	
V6	$(1\bar{1}02)[\bar{1}101]$	

3 Results

3.1 Initial microstructures

As are depicted in Figs. 2(a–c), the inverse pole figure (IPF) maps of the Mg−Y sheets along the normal direction (ND) exhibited similar initial microstructures of fully recrystallized and equiaxed grains with almost uniform grain size. In addition, the microstructures were twin-free at the present EBSD step size. The equivalent grain diameters of Mg−0.5Y, Mg−1Y and Mg−5Y sheets were (5.0±2.3), (6.0±2.5) and (7.2±2.7) μm, respectively (Figs. 2(d−f)).

As illustrated in Figs. 2(g–i), with the increase of Y content, the texture characteristics were remarkably weakened regardless of intensity and distributions. The texture in Mg−0.5Y exhibited a weakened basal texture (Fig. 2(g)). The maximum basal pole of the {0001} pole figure (PF) tilted by 10° from ND to ED, the intensity of which was 17 mrd. For the IPF map, the maximum pole was around $\langle 10\bar{1}0\rangle$. In the Mg−1Y sheet, the basal texture was further weakened (Fig. 2(h)). The tilt angle of the maximum basal pole in PF to ED increased to about 30°, and its intensity was reduced to 15 mrd. The $\langle 20\bar{2}1\rangle$ of most grains was parallel to ED. Adding 5% Y to the matrix notably weakened the texture and led to a typical rare earth texture (Fig. 2(i)). The basal pole in PF split along ED and tilted by ~45°, the intensity of which was reduced to 4.9 mrd.

3.2 Mechanical behavior

The engineering stress−engineering plastic strain curves of the Mg−Y sheets under the ED tensile and compressive testing with the corresponding mechanical properties are illustrated in Fig. 3. As shown in Fig. 3, with the increase of Y content, the mechanical behavior of Mg−Y sheets

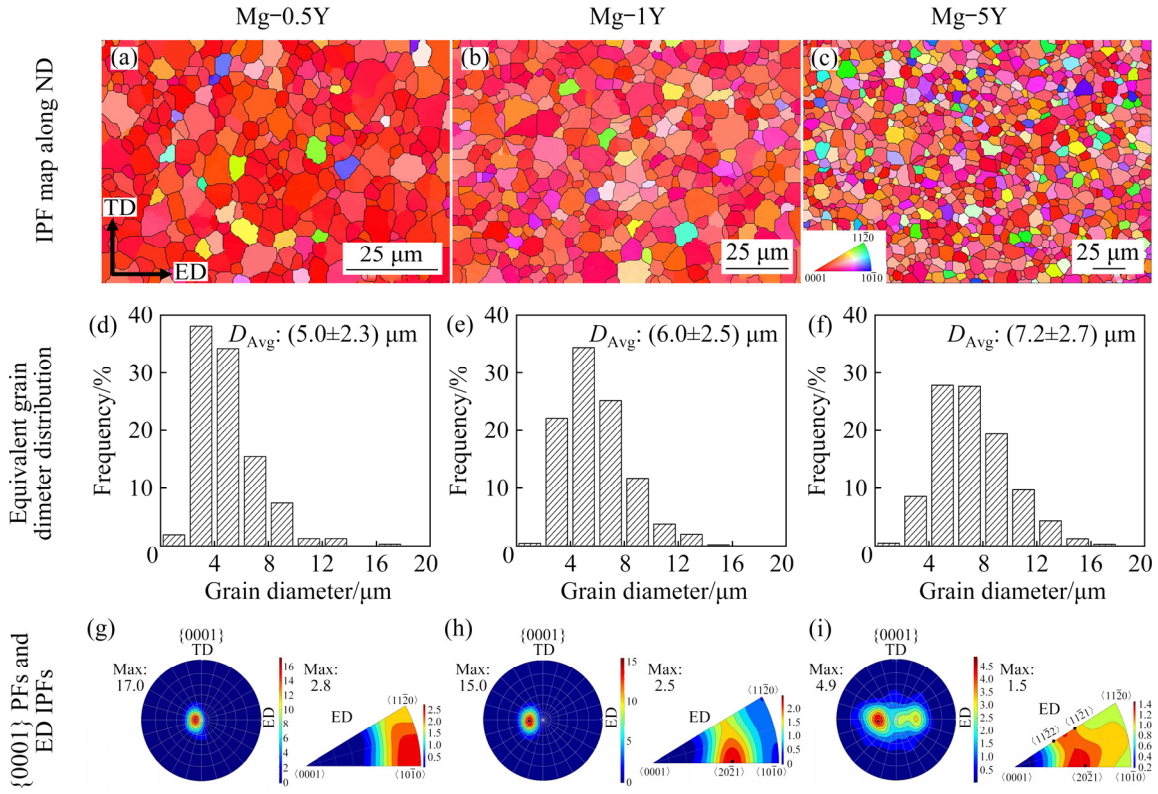

Fig. 2 Initial microstructures (a−c), equivalent grain diameter distribution (d−f), and {0001} pole figures (PFs) and ED IPFs (g−i) of as-extruded Mg−xY (x=0.5, 1, 5, wt.%) sheets on ED−TD plane

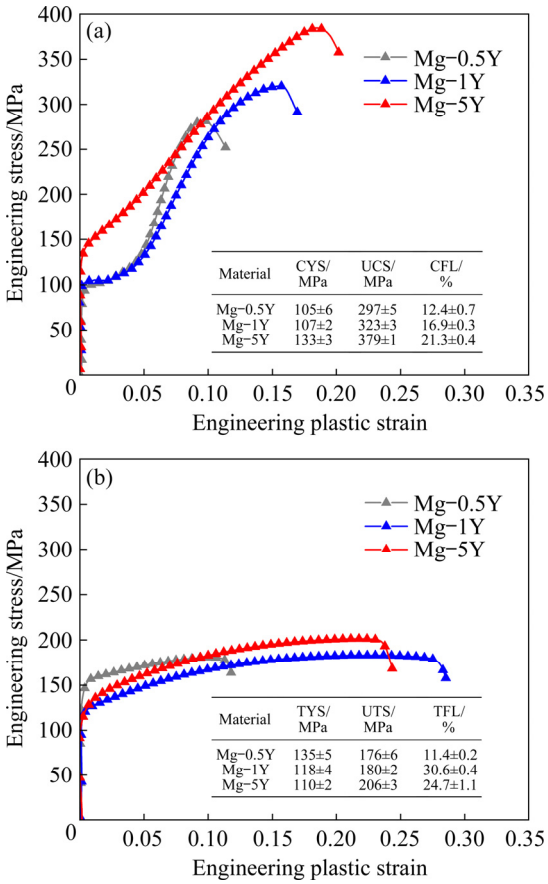

Fig. 3 Engineering stress–engineering plastic strain curves of Mg−0.5Y, Mg−1Y and Mg−5Y sheets under compression (a) and tension (b) along ED with compressive/tensile mechanical properties inserted

changed to different extents. For the Mg−Y compression specimens (Fig. 3(a)), the compressive yield stress (CYS), ultimate compressive stress (UCS), and compressive fracture elongation (CFL) increased simultaneously with the increase of Y content. The CYS, UCS, and CFL of Mg−5Y were 27%, 36%, and 72% higher than those of Mg−0.5Y, respectively. The compressive mechanical behavior curves exhibited a gradually unobvious concave-up (sigmoidal) tendency, which hinted an alteration of the twinning-dominated deformation mechanism [37−39]. For all the Mg−Y samples under tension, the mechanical behavior curves showed a characteristic of concave-down (Fig. 3(b)). Furthermore, it is worth noting that, adding Y to the matrix led to decreased tensile yield stress (TYS). It can be deduced that the competitive effect of solid solution strengthening and the weakened texture-induced geometric softening of basal slip, the dominant deformation mechanism under tension, may account for the results [29].

3.3 Twinning behavior after compression

The representative microstructures of the Mg−Y sheets as well as the corresponding twin boundary maps and texture characteristics after compressive testing to failure are shown in Fig. 4. As shown in Figs. 4(a, c), the Mg−0.5Y compressive specimen underwent dramatic twinning, which was consistent with the great texture change compared with the texture before loading (Figs. 2(a, g)). A detailed statistical twin analysis was carried out using the method previously mentioned, and statistical information is summarized in Table 2. In the studied area containing ~200 grains, a total of 248 twins were identified. Eight-seven percent of the grains were twinned, and the twinned area fraction was up to 0.81. The twinned grain boundary fraction was 0.64. Note that the twin boundary fraction of 0.64 here was just limited to the identified twin boundaries because there were many grains extremely twinned over the whole grain. As summarized in Tables 3 and 4, of all twins, 98.3% (area fraction) were identified as TTWs. The texture feature that the *c*-axis of the most grains deviated 90° from ND to ED was consistent with the TTW dominant twinning behavior (Fig. 4(c)).

In the observation area of the Mg−1Y compressive sample containing 389 grains in Fig. 4(d), a total of 388 twins were identified, with the slightly decreased twinned area fraction of 0.78 compared with Mg−0.5Y. Eighty-one percent of the grains were twinned, and the fraction of the twinned grain boundary was 0.46. As summarized in Tables 3 and 4, the $\{10\bar{1}2\}$ TTWs accounted for 95.5% (area fraction) of all twins observed in the Mg−1Y compressive sample, which was basically in agreement with this significant texture change pre and post loading (Figs. 2(h) and 4(f)).

With the increase of Y content to 5%, the twinning activity was less pronounced (Figs. 4(g−i)). To ensure statistics, more grains were included in the experimental observation for both Mg−5Y compressive and tensile samples. A total of 684 grains were observed under ED compression condition for the Mg−5Y sheet, among which 187 twins were identified. The twinned grain fraction was reduced to 0.20, and the twinned area fraction was 0.12. The twinned grain boundary fraction decreased to 0.31, which could be also found from Fig. 4(h). The predominance of $\{10\bar{1}2\}$ TTWs

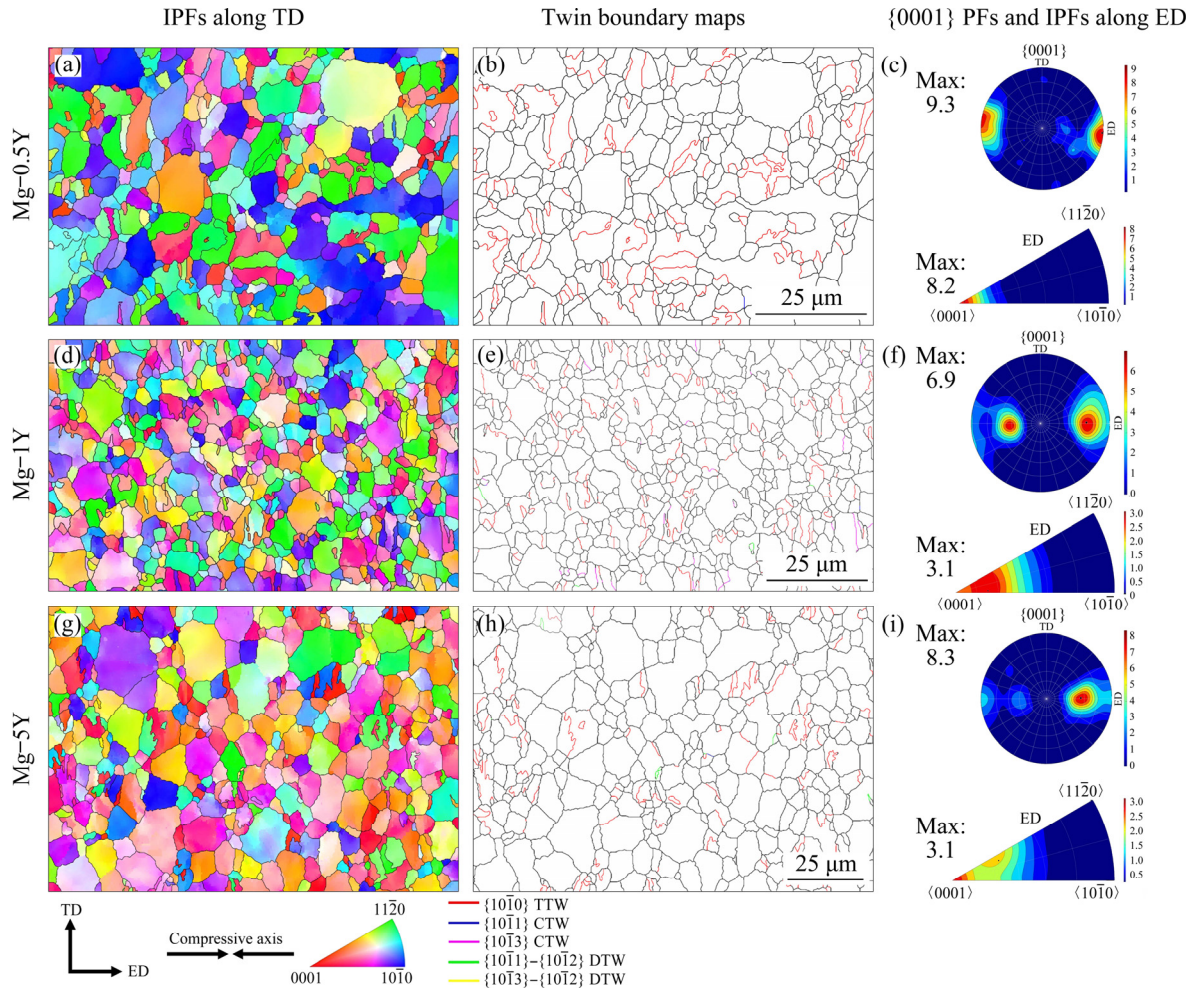

Fig. 4 Twinning characteristics of Mg−Y sheets after compression to fracture

Table 2 Statistical information of twinning activity for Mg−*x*Y (*x*=0.5, 1, 5, wt.%) sample deformed to fracture in compression (C) and tension (T)

Information	Feature	Mg−0.5Y−C	Mg−1Y−C	Mg−5Y−C	Mg−1Y−T	Mg−5Y−T
Area	Number of grains	200	389	684	334	1084
	Number of grain boundaries	492	987	1752	893	2984
Twin	Number of twins	248	388	187	42	112
	Average twin number per grain	1.25	1	0.27	0.13	0.1
	Twinned area fraction	0.81	0.78	0.12	0.06	0.04
	Twinned grain fraction (grains with at least one twin/total grains)	0.87	0.81	0.2	0.08	0.07
	Twinned grain boundary fraction (boundaries connected to at least one twin/total boundaries)	0.64	0.46	0.31	0.14	0.09

was still significant, and the relative area fraction was as high as 95.8%.

The morphology statistics of the TTWs in Mg−Y compression specimens are shown in Fig. 5. For Mg−0.5Y specimen, the identified TTWs exhibited an average twin length of (5.3±3.6) μm and an average true twin thickness of (1.2±1.3) μm (the true twin thickness was equal to the measured twin thickness projected on the ED−TD observation plane multiplied by the cosine of the angle between the normal of the twin plane (k_1) and the normal of the observed plane [40]) (Figs. 5(a, d)). Increasing

Table 3 Statistical information of activated twin modes for Mg−Y sample deformed to fracture in compression and tension

Twin mode	Compression			Tension	
	Mg−0.5Y	Mg−1Y	Mg−5Y	Mg−1Y	Mg−5Y
$\{10\bar{1}2\}$ TTW	241	366	173	37	107
$\{10\bar{1}1\}$ CTW	1	2	2	2	−
$\{10\bar{1}3\}$ CTW	−	17	−	−	−
$\{10\bar{1}1\}-\{10\bar{1}2\}$ DTW	−	3	9	3	−
$\{10\bar{1}3\}-\{10\bar{1}2\}$ DTW	−	−	−	−	−
$\{10\bar{1}2\}-\{10\bar{1}2\}$ DTW	6	−	−	−	5
TTW−$\{10\bar{1}1\}-\{10\bar{1}2\}$ DTW tertiary twin	−	−	3	−	−
Total	248	388	187	42	112

Table 4 Area fraction and relative area fraction of activated twins for different twin modes observed in Mg−Y compressive and tensile samples

Twin mode	Area fraction (particular twin area/total measured area)/%					Relative area fraction (particular twin area/total twin area)/%				
	Compression			Tension		Compression			Tension	
	Mg−0.5Y	Mg−1Y	Mg−5Y	Mg−1Y	Mg−5Y	Mg−0.5Y	Mg−1Y	Mg−5Y	Mg−1Y	Mg−5Y
$\{10\bar{1}2\}$ TTW	79.3	74.5	11.9	5	3.6	98.3	95.5	95.8	89.3	97
$\{10\bar{1}1\}$ CTW	0.3	0.3	0.4	0.3	−	0.3	0.4	3.2	5.9	−
$\{10\bar{1}3\}$ CTW	−	2.3	−	−	−	−	2.9	−	−	−
$\{10\bar{1}1\}-\{10\bar{1}2\}$ DTW	−	0.9	0.1	0.3	−	−	1.2	0.8	4.6	−
$\{10\bar{1}3\}-\{10\bar{1}2\}$ DTW	−	−	−	−	−	−	−	−	−	−
$\{10\bar{1}2\}-\{10\bar{1}2\}$ DTW	1.1	−	−	−	0.1	1.4	−	−	−	3
TTW−$\{10\bar{1}1\}-\{10\bar{1}2\}$ DTW tertiary twin	−	−	0.03	−	−	−	−	0.2	−	−
Total	80.7	78	12.5	5.6	3.7	100	100	100	100	100

Y content to 1% and 5% had little effect on the average twin length and average true twin thickness of identified TTWs compared with Mg−0.5Y specimen. Note that only TTWs that can be identified were included here.

The detailed activated TTW variants and corresponding m values of Mg−Y compressive samples are illustrated in Fig. 6. As shown in Fig. 6(a), only 17% of the identified TTWs in Mg−0.5Y had m values >0.4, and 25% of them had negative m values. In other words, the widely accepted Schmid law failed to effectively explain the twin variant selection in this case. To indicate how close the active m was to the maximum m among the six possible TTW variants, a normalized Schmid factor (m_{nor}) was proposed in this work, which is defined as $m_{nor}=(m-m_{min})/2(m_{max}-m_{min})$. As shown in Fig. 6(d), the identified TTWs in Mg−0.5Y were characterized by 76% m_{nor} values >0.4 and only 10% m_{nor} values <0.2. It can be concluded that the proposed m_{nor} can predict the TTW variant selection more effectively. As depicted in Fig. 6(b), for Mg−1Y, the activated TTWs were characterized by relatively low m values, with only 2% of twins exhibiting m values larger than 0.4, and 26% of twins exhibiting negative m values. After normalization, 84% of the twins had m_{nor}>0.4 (Fig. 6(e)). With the increase of Y content to 5%, the m values were evenly distributed over a wide range from about −0.3 to 0.5 (Fig. 6(c)). After normalization, 90% of TTWs exhibited m_{nor}>0.4 (Fig. 6(f)).

Generally speaking, under the compression condition of Mg−Y sheets, the twinning activity

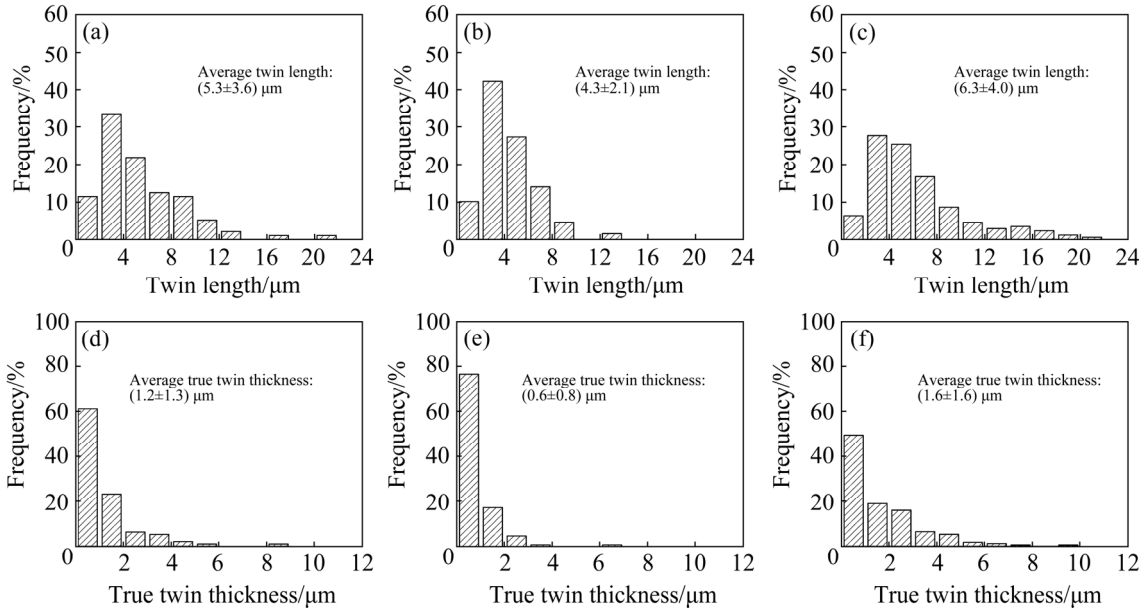

Fig. 5 Distribution of twin length (a−c) and true twin thickness (d−f) for all identified TTWs in compression specimens: (a, d) Mg−0.5Y; (b, e) Mg−1Y; (c, f) Mg−5Y

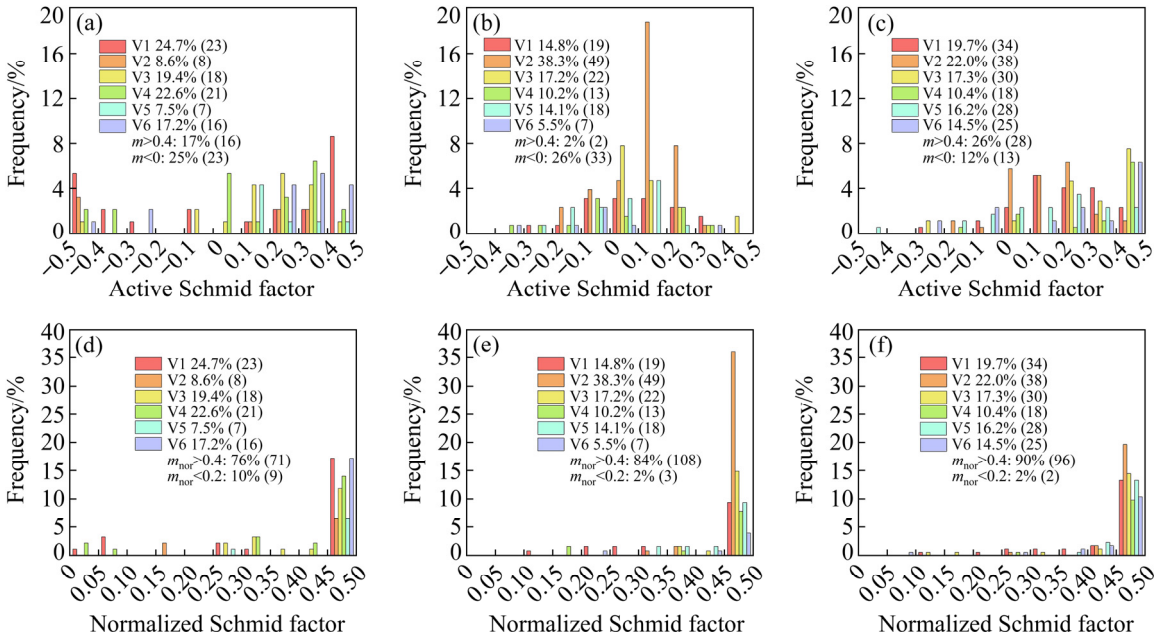

Fig. 6 Frequency of twin variants activated in Mg−Y compressive specimens and m values distributions: (a, d) Mg−0.5Y; (b, e) Mg−1Y; (c, f) Mg−5Y

decreased with the increase of Y content, which was reflected in the reduction of the twinned area fraction, twinned grain fraction, average twin number per grain, and twinned grain boundary fraction. Besides, twin variant selection can be better explained by m_{nor} with the increase of Y content. The fraction of twins with m_{nor}>0.4 significantly increased from 76% in the Mg−0.5Y sheet to 90% in the Mg−5Y sheet (Figs. 6(d, e, f)).

In addition, it should be noted that when Y content increased to 1% and above, twinning modes began to abound. Different from Mg−0.5Y, additional $\{10\bar{1}1\}$ CTWs, $\{10\bar{1}3\}$ CTWs, double twins ($\{10\bar{1}1\}-\{10\bar{1}2\}$ DTWs), and even tertiary twins (TTW − $\{10\bar{1}1\}-\{10\bar{1}2\}$ DTW) were observed in Mg−1Y and/or Mg−5Y (Figs. 4 and 7). The detailed statistical information of these CTWs, DTWs, and tertiary twins are provided in Tables 3 and 4.

Figure 7 demonstrates the tertiary twins in the Mg−5Y compression sample. By taking grain labeled 100-P in Fig. 7(a) as an example, the formation process of the tertiary twins was as follows: first, the primary TTW labeled 99-V2 ($(01\bar{1}2)[0\bar{1}11]$, m=0.47) was produced in the parent grain, and then the double twin ($\{10\bar{1}1\}-\{10\bar{1}2\}$ DTW) numbered 109-V2→ $\{10\bar{1}1\}-\{10\bar{1}2\}$ DTW was developed in the primary TTW. The visualized orientation and formation procedure for the TTW−$\{10\bar{1}1\}-\{10\bar{1}2\}$ DTW tertiary twins including the rotation angles and axes, the twinning plane (k_1) / direction (η_1), and the m value of the primary twin are also provided in Fig. 7(c). The similar TTW−$\{10\bar{1}1\}-\{10\bar{1}2\}$ DTW tertiary twins (195-V4 → $\{10\bar{1}1\}-\{10\bar{1}2\}$ DTW, 187-V4 → $\{10\bar{1}1\}-\{10\bar{1}2\}$ DTW) were observed in the parent grain 192-P, as shown in Figs. 7(d–f). It was worth noting that six uncommon $\{10\bar{1}2\}-\{10\bar{1}2\}$ DTWs were activated in the Mg−0.5Y compressive specimen, one of which is shown in Figs. 8(a–c). First, 163-V3 ($(\bar{1}102)[1\bar{1}01]$, m=−0.01) primary $\{10\bar{1}2\}$ TTW was formed in parent grain 173-P, and then, the secondary V3 variant ($(\bar{1}102)[1\bar{1}01]$, m=0.22) and V4 variant ($(\bar{1}012)[10\bar{1}1]$, m=0.13), designated as 134-V3→V3 and 131-V3→V4, were developed in the primary 163-V3 domain. It is worth noting that the m value of primary twin 163-V3 was negative, while the secondary twins all exhibited relatively high and positive m values (Fig. 8(c)).

It was known that the activity of these additional twinning modes was low and limited, in terms of twin number and twin area fraction, compared to those of TTW, as shown in Tables 3 and 4. For example, the relative area fraction (particular twin area/total twin area) for TTWs was always larger than 95% for all the Mg−Y alloys studied under compression. Thus, a detailed analysis was mainly focused on the TTWs.

3.4 Twinning behavior after tension

The typical microstructure, twin boundary map, and the texture characteristics of Mg−1Y and Mg−5Y sheets after ED tensile deformation to fracture are shown in Fig. 9. In the observation area of the Mg−1Y tensile sample shown in Fig. 9(a), of all 334 grains, 42 twins were observed. The statistical information of twinning is summarized in Tables 2−4. The total twinned area fraction was 0.06, and the proportion of twinned grains was 0.08. The twinned grain boundary fraction was 0.14. Of all the twins, 89.3% (area fraction) were TTWs.

For the Mg−5Y tensile specimen, a large area containing 1084 grains was observed, and a representative microstructure patch is shown in Fig. 9(d). The twinning activity for Mg−5Y ED tension was further reduced compared with that of Mg−1Y. In the observed area, 112 twins were

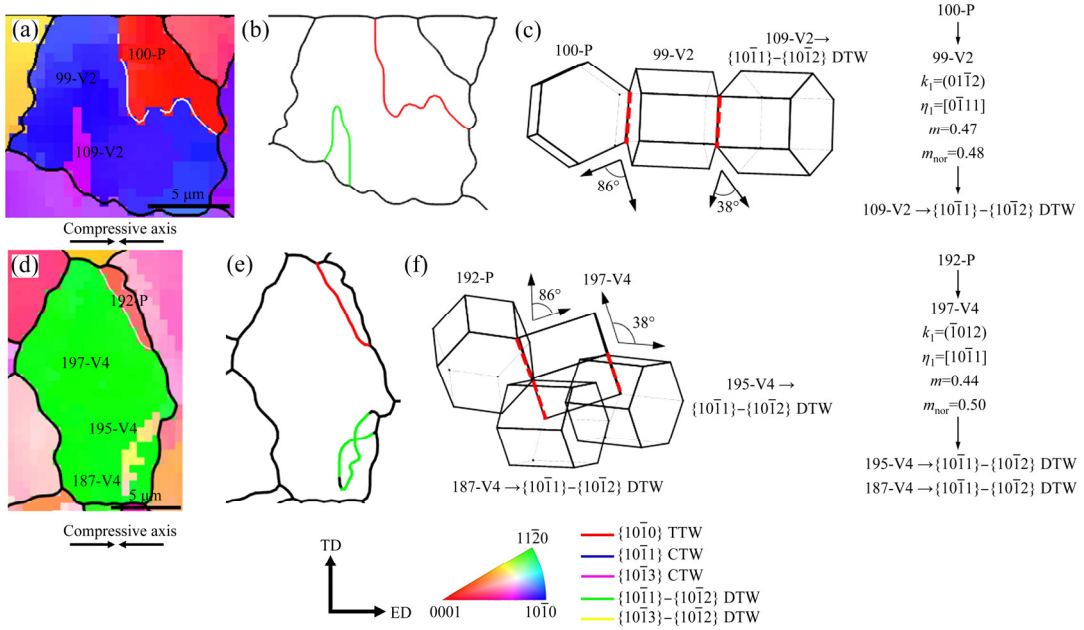

Fig. 7 Diagrams of tertiary twins (TTW−$\{10\bar{1}1\}-\{10\bar{1}2\}$ DTW) in Mg−5Y compressive specimen: (a, d) IPF maps; (b, e) Boundary maps; (c, f) Visualized misorientation relationship among parent grains, primary twins, and tertiary twins

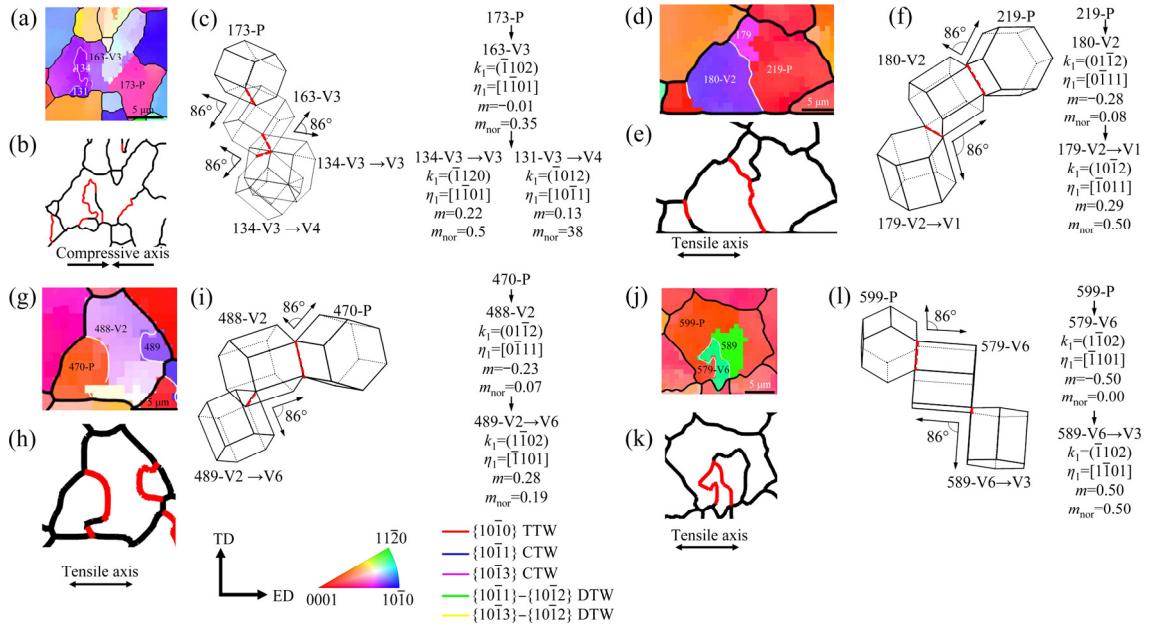

Fig. 8 Diagrams of $\{10\bar{1}2\}-\{10\bar{1}2\}$ DTWs in Mg−0.5Y compressive (a−c) and Mg−5Y tensile (d−l) specimens: (a, d, g, j) IPF maps; (b, e, h, k) Boundary maps of corresponding area; (c, f, i, l) Visualized misorientation relationship among parent grains, primary twins and secondary twins

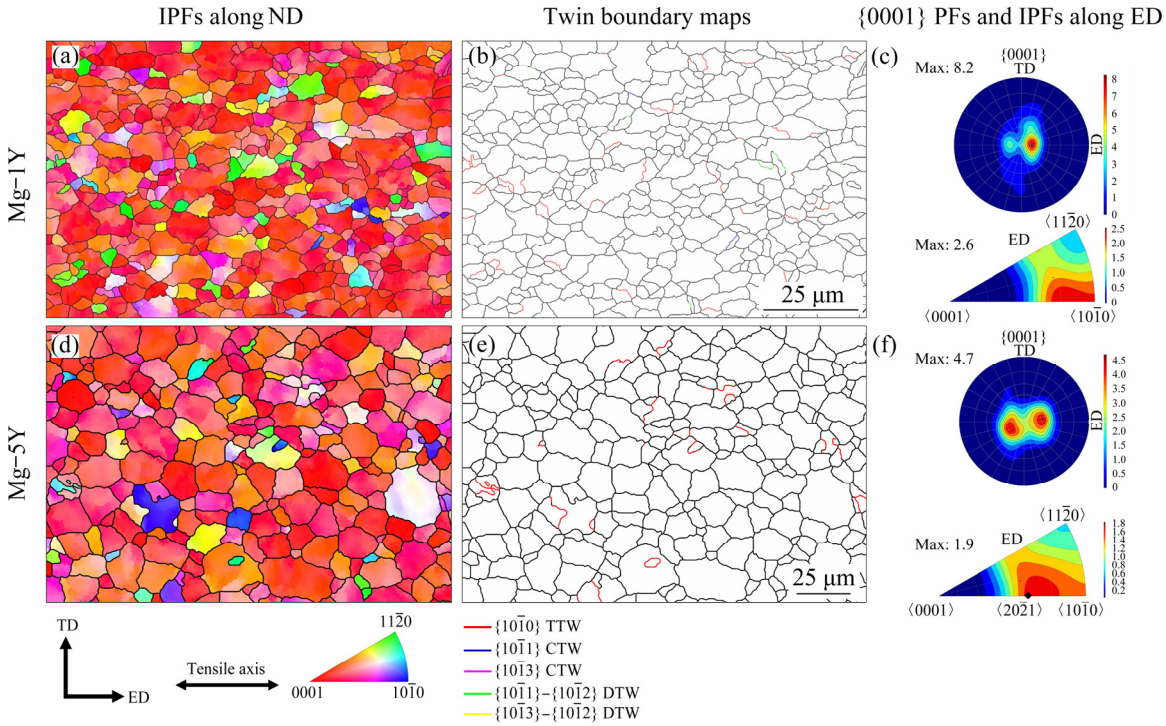

Fig. 9 Microstructures of Mg−Y sheets after tensile testing to fracture

identified in total. The twinned area fraction decreased to 0.04, and the twinned grain fraction was 0.07. The twinned grain boundary fraction was as low as 0.09. The low twinning activity was in agreement with the almost invariable texture pre and post loading, as shown in Figs. 2(i) and 9(f). Of all twins identified in the studied area, the TTW was still the dominant mode which accounted for a relative area fraction of 97.0%.

Since the TTWs were still dominant after tensile deformation, further analyses of the TTWs were carried out. Figure 10 shows the twin length

and true twin thickness distribution for the identified TTWs in Mg−Y tension specimens. The average length and an average true twin thickness for the TTWs in Mg−1Y were (4.4±1.5) μm and (1.7±1.1) μm, respectively (Figs. 10(a, c)). For the TTWs in Mg−5Y, the average twin length and true twin thickness were (8.0±3.6) μm and (3.1±2.3) μm, respectively (Figs. 10(b, d)).

The detailed activated variants and m value statistics of TTWs in Mg−Y tension specimens are shown in Fig. 11. As illustrated in Fig. 11(a), the TTWs in Mg−1Y were characterized by relatively low m values, with 32% of twins exhibiting m<0. After normalization, 92% of twins had m_{nor}>0.4. As shown in Fig. 11(b), for Mg−5Y tension specimen, the m values of the TTWs were distributed over a wide range and 50% of twins exhibited m<0. Only 45% of twins had m_{nor}>0.4, and the fraction of twins with m_{nor}<0.2 was as high as 47%. Compared with Mg−1Y tension, the twin variant selection was less consistent with the Schmid law, even after normalization.

In addition to the TTWs, five $\{10\bar{1}2\}-\{10\bar{1}2\}$ DTWs were identified in the observation area of the Mg−5Y tensile specimen. Three examples are shown in Figs. 8(d−l), and the formation process is described in Fig. 8(a). As same as the $\{10\bar{1}2\}-\{10\bar{1}2\}$ DTWs previously described in Figs. 8(a–c), through the process of secondary twinning, the m values changed from the negative of the primary twins to the positive of the secondary twins.

To be summarized, the twinning activity reduced as the Y content increased both in tension and compression samples. However, there were differences in twinning behavior between tension and compression. Firstly, the twinning activity under tension was significantly lower than that under compression. Secondly, compared with tension, with the increase of Y content, the twinning modes became more abundant under compression, and the twin variant selection can be better explained by m_{nor}.

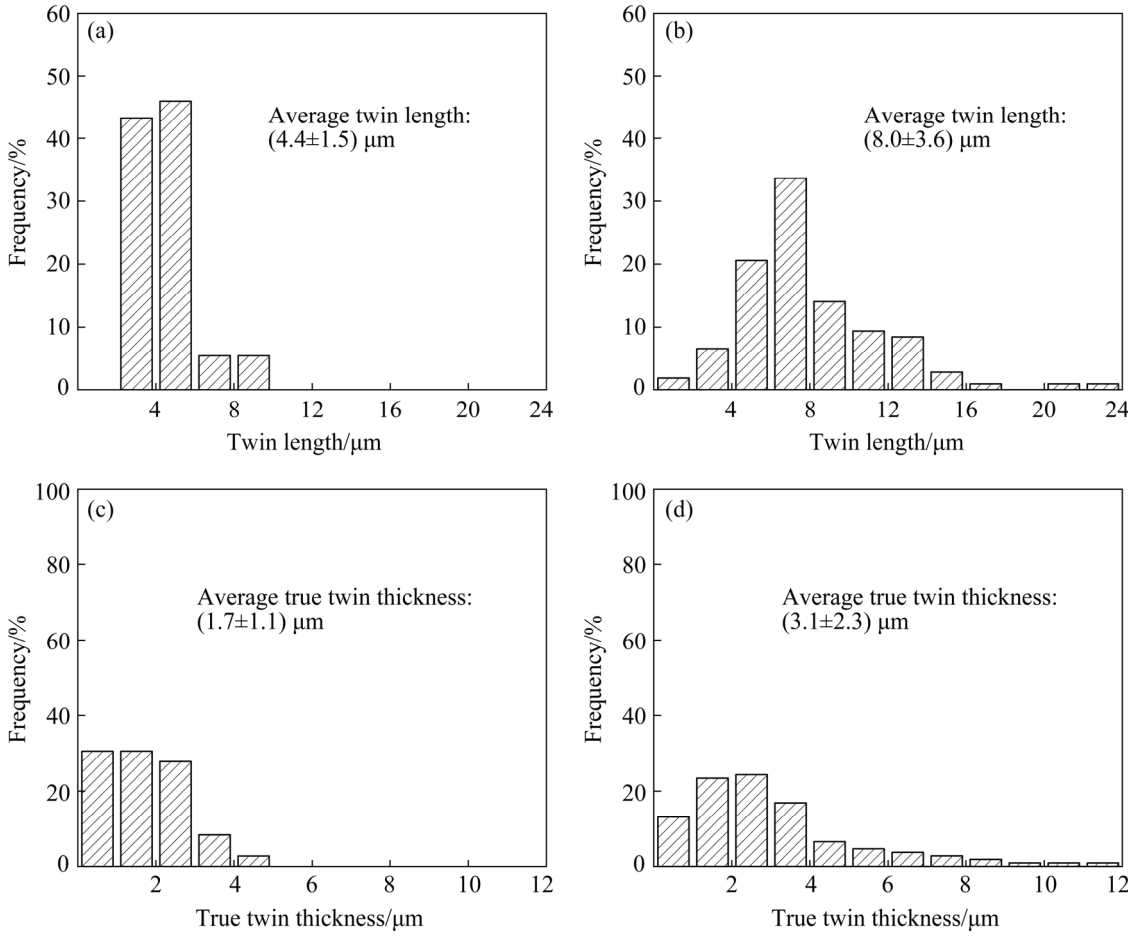

Fig. 10 Distribution of twin length (a, b) and true twin thickness (c, d) for all identified TTWs in tension specimens: (a, c) Mg−1Y; (b, d) Mg−5Y

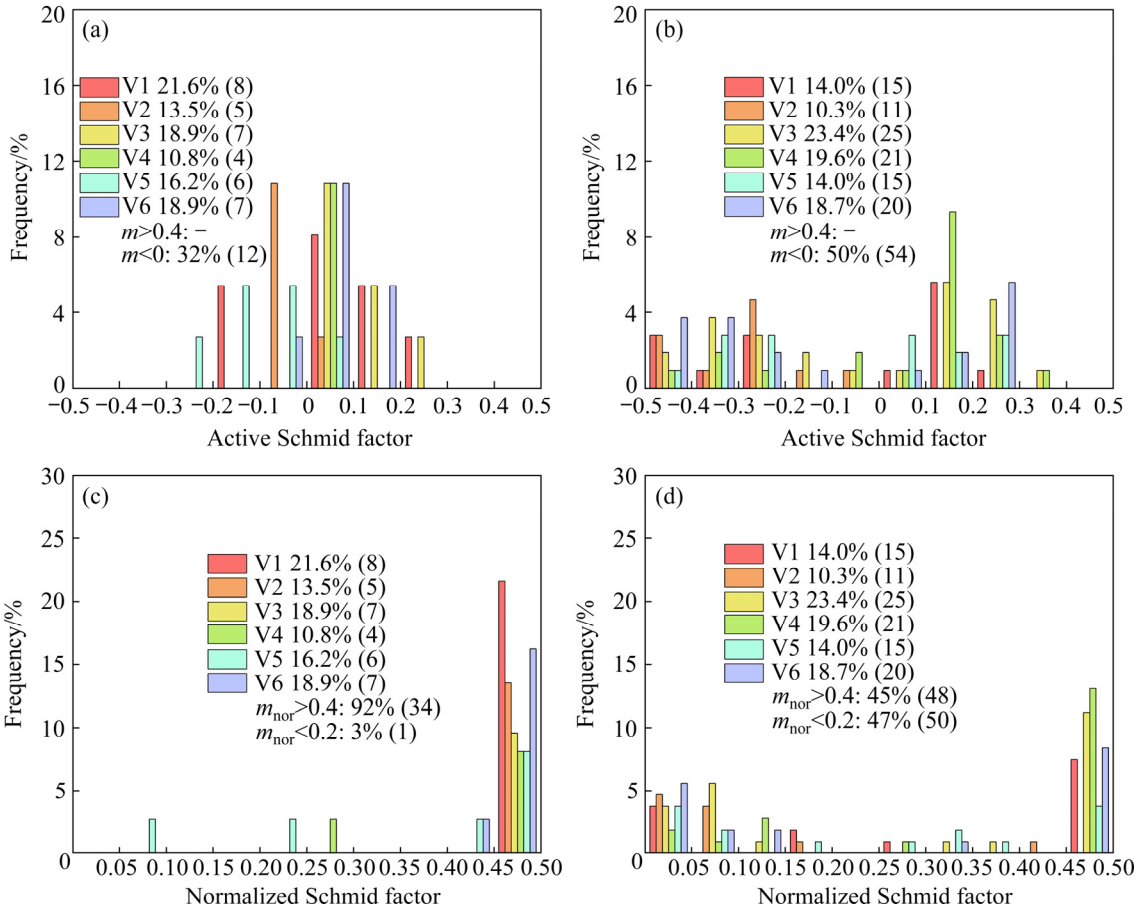

Fig. 11 Frequency of twin variants activated in Mg−Y tension specimens currently studied and *m* value distributions: (a, c) Mg−1Y; (b, d) Mg−5Y

4 Discussion

4.1 Non-Schmid twinning behavior

The average Schmid factors of possible $\{10\bar{1}2\}$ TTWs and $\{10\bar{1}1\}$ CTWs under the compression and tension for the studied materials are shown in Fig. 12 to illustrate texture effects on the twinning behavior, in which both positive and negative *m* values were considered. The TTWs were less favorably orientated as Y content increased under compression loading condition, and under tension loading, the average *m* values of TTWs increased slightly but were always less than 0, which was basically consistent with the observation, especially in terms of relative area fraction, as given in Table 4. However, it is worth noting that TTWs always dominated, even in an extremely unfavorable orientation, such as tension for all materials studied and compression for Mg−5Y, in which the average *m* values of TTWs were negative.

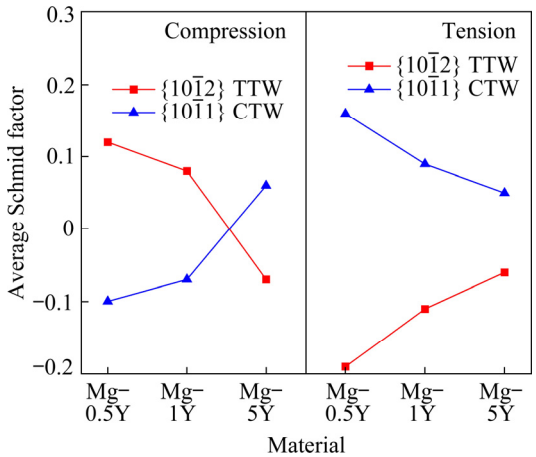

Fig. 12 Average Schmid factor for possible TTWs and CTWs under compression and tension loading

The above studies on TTWs in the Mg−Y tension/compression specimens demonstrated that the activation of TTWs could not be well explained by the widely accepted Schmid law. Specifically, for Mg−Y compression specimens, the fraction of anomalous TTWs with negative *m* values was as high as 25%, 26% and 12%, respectively

(Figs. 6(a−c)). Besides, as shown in Figs. 11(a, b), up to 32% and 50% of all the TTWs in Mg−1Y and Mg−5Y tension samples in the studied areas were anomalous twins. Similar results have also been reported in previous work of pure titanium performed under RD compression [21] or pure Mg under ED tension loading [23] as well as magnesium alloys such as AZ31 under RD compression [22] and tension [41].

Several possible explanations have been proposed, but a full understanding of this non-Schmid behavior has not been achieved yet. Given that a Schmid factor (m) in completely geometric type was employed here, i.e. the local and global stress state is regarded to be identical, and the TTWs with low or negative m values may be formed to coordinate the local stress state which may deviate from or even be contrary to the global stress state due to deformation heterogeneity. The previous deformation heterogeneity study in terms of IGM and GND density distributions for pure Mg [23] and digital image correlation (DIC) results carried out on magnesium alloy WE43 [42] and a nickel-based superalloy Hastelloy X [43] indirectly or directly indicated that local strain can even be contrary to macroscopically applied strain.

In this study, the proportion of the anomalous TTWs with m<0 in the Mg−Y sheets is found to slightly increase with the increasing maximum m values for the basal slip in the corresponding parent grains during ED compression, and increase with the increasing maximum m values of prismatic slip in the parent grains during ED tension, as illustrated in Fig. 13. The above results indicated that the anomalous TTWs formation and variant selection may be intimately related to the basal slip and prismatic slip, which was supported by the results of others. Previously, KOIKE et al [41] also found that the TTWs tendency increased with increasing m values of the basal slip, but it was in textured AZ31 Mg alloy under RD tension. Recently, DELLA VENTURA et al [44] performed an in situ micro-tensile loading on pure Mg along the directions completely parallel to the c-axis and at an angle of 5° with the c-axis. Their results clearly indicated that the activation of basal slip in 5° tensile loading to the c-axis triggered a large amount of TTWs nucleation, while limited twin formation was identified when loading completely parallel to the c-axis. In addition, JEONG et al [45] found that the prismatic slip pile-up resulted in the local stress concentration source which was favorable for the twin nucleation during $[2\bar{1}\bar{1}0]$ compression in Mg single crystal by in-situ transmission electron microscopy (TEM).

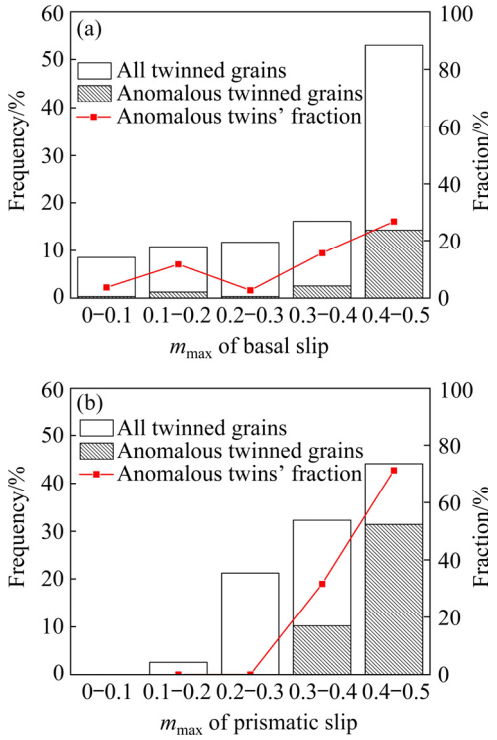

Fig. 13 Correlation between proportion of anomalous TTWs with m<0 and maximum Schmid factor (m_{max}): (a) Basal slip in corresponding parent grains for Mg−Y compression specimens; (b) Prismatic slip in corresponding parent grains for Mg−Y tension specimens

4.2 Impact of alloying content on twinning activation mechanism

Another important finding in the present research was that under tensile loading, the twin variant selection was less consistent with Schmid law as the Y content increased. Especially for the Mg−5Y tensile specimen, the m values of the TTWs were almost randomly distributed between −0.5 and 0.4 (Fig. 11(b)). In other words, with the increase of Y content, the twin variant selection became more stochastic in Mg−Y tension sample. HU et al [46] also found that an increase of Al content in Mg−Al alloys promoted the stochastic twin variant selection process on the atomic level using high-throughput atomistic simulations. They attributed the random twin variant selection to the stochastic nucleation event and twinning disconnections' pinning or depinning of Al atoms.

It should be aware that the above results are not the full story, and loading conditions also played an important role in it. The variant selection of TTWs became more consistent with Schmid law after normalization with increasing Y content in the studied Mg−Y compressive specimens (Fig. 6). Therefore, the role the alloying played in the process of twin variant selection still needs to be better understood.

On the other hand, as shown in Tables 3 and 4, when the Y content increased to 1%, the number of activated twin modes increased significantly, and a few complex $\{10\bar{1}2\}-\{10\bar{1}2\}$ DTWs and TTW−DTW tertiary twins were activated in Mg−5Y specimens (Figs. 7 and 8). That is to say, the activated twin types increased with the increase of Y alloying element content. Note that these additional twinning modes only accounted for a small part, in terms of twin number and relative twinning area fraction, as shown in Tables 3 and 4, so there was not too much detailed analysis of them. STANFORD et al [47] reported that with the Y content increasing from 5% to 10%, the common $\{10\bar{1}2\}$ twin was significant hardening and the less common $\{11\bar{2}1\}$ tension twins were identified. One possible reason they suggested is that the larger Y atomic radius compared with Mg strengthens the $\{10\bar{1}2\}$ twins, making $\{11\bar{2}1\}$ tension twin, which is less sensitive to Y content, more prominent in Mg−10Y. HE et al [48] found that the dominant twin mode changed from $\{10\bar{1}2\}$ twinning to $\{11\bar{2}1\}$ tension twinning with the addition of more Gd to Mg and proposed that the larger Gd solute atoms result in the decrease of $\{11\bar{2}1\}$ twin boundary energy. In addition, it has been reported that the alloying solute concentration in AZ series Mg alloys has an important effect on the process of detwinning, compared with pure magnesium, the secondary twinning is more likely to occur in AZ31 and AZ91 alloys, and the higher the alloying content is, the more significant it is.

5 Conclusions

(1) The twinning activity decreased with the increase of Y content, which was reflected in the reduction of the twinned area fraction, twinned grain fraction, average twin number per grain and twinned grain boundary fraction. Twinning activity under compression was always higher than that under tension.

(2) The effect of Y content on the twin variant selection under compression and tension was different. The twin variant selection was more stochastic and less consistent with the Schmid law for tension. In the Mg−1Y tension specimen, 92% of the TTWs in the studied area exhibited $m_{nor}>0.4$, while for Mg−5Y, this fraction decreased to 45%, and 47% of the TTWs exhibited $m_{nor}<0.2$. However, under compression loading condition, the twin variant selection can be better explained by the m_{nor} values with increasing Y content. The fraction of the TTWs with $m_{nor}>0.4$ increased from 76% in the Mg−0.5Y sheet to 90% in the Mg−5Y sheet.

(3) The other effect of increasing Y content on twinning was to promote the activation of more abundant and complex twinning modes.

(4) It was found that the proportion of the anomalous twins with $m<0$ was closely related to the maximum Schmid factor (m_{max}) of slip in the corresponding parent grains. The anomalous twins' fraction in the Mg−Y samples was found to slightly increase with increasing m_{max} values of basal slip in the corresponding parent grains under ED compressive loading, and increase with increasing m_{max} values of prismatic slip in the corresponding parent grains under ED tension.

Acknowledgments

This work was supported by the National Natural Science Foundation of China (Nos. 51401172 and 51601003), Fundamental Research Funds for the Central Universities, China (No. 2682020ZT114) and open funding of International Joint Laboratory for Light Alloys (MOE), Chongqing University, China. We would like to thank the Analytical and Testing Center of Southwest Jiaotong University for assistance with SEM and EBSD characterization.

References

[1] POLLOCK T M. Weight loss with magnesium alloys [J]. Science, 2010, 328(5981): 986−987.

[2] WANG X J, XU D K, WU R Z, CHEN X B, PENG Q M, JIN L, XIN Y C, ZHANG Z Q, LIU Y, CHEN X H, CHEN G, DENG K K, WANG H Y. What is going on in magnesium alloys? [J]. Journal of Materials Science & Technology, 2018, 34(2): 245−247.

[3] ZHANG Zhi, ZHANG Jing-huai, XIE Jin-shu, LIU Shu-juan, HE Yu-ying, GUAN Kai, WU Rui-zhi. Developing a low-alloyed fine-grained Mg alloy with high strength-

ductility based on dislocation evolution and grain boundary segregation [J]. Scripta Materialia, 2022, 209: 114414.

[4] ZHANG Zhi, ZHANG Jing-huai, XIE Jin-shu, LIU Shu-juan, HE Yu-ying, WANG Ru, FANG Da-qing, FU Wei, JIAO Yun-lei, WU Rui-zhi. Significantly enhanced grain boundary Zn and Ca co-segregation of dilute Mg alloy via trace Sm addition [J]. Materials Science and Engineering A, 2022, 831: 142259.

[5] QIAN Qi, LIU Zheng-qing, JIANG Yong, WANG Yi-ren, AN Xing-long, SONG Min. Basal stacking fault induced twin boundary gliding, twinning disconnection and twin growth in hcp Ti from the first-principles [J]. Transactions of Nonferrous Metals Society of China, 2021, 31(2): 382−390.

[6] TANG Xiao-zhi, ZHANG Hui-shi, GUO Ya-fang. Atomistic simulations of interactions between screw dislocation and twin boundaries in zirconium [J]. Transactions of Nonferrous Metals Society of China, 2018, 28(6): 1192−1199.

[7] XU Hong-lu, SU Xiao-ming, YUAN Guang-yin, JIN Zhao-hui. Primary and secondary modes of deformation twinning in HCP Mg based on atomistic simulations [J]. Transactions of Nonferrous Metals Society of China, 2014, 24(12): 3804−3809.

[8] CHRISTIAN J W, MAHAJAN S. Deformation twinning [J]. Progress in Materials Science, 1995, 39(1/2): 1−157.

[9] FRYDRYCH K, MAJ M, URBAŃSKI L, KOWALCZYK-GAJEWSKA K. Twinning-induced anisotropy of mechanical response of AZ31B extruded rods [J]. Materials Science and Engineering A, 2020, 771: 138610.

[10] FEATHER W G, GHORBANPOUR S, SAVAGE D J, ARDELJAN M, JAHEDI M, MCWILLIAMS B A, GUPTA N, XIANG Chong-chen, VOGEL S C, KNEZEVIC M. Mechanical response, twinning, and texture evolution of WE43 magnesium−rare earth alloy as a function of strain rate: Experiments and multi-level crystal plasticity modeling [J]. International Journal of Plasticity, 2019, 120: 180−204.

[11] FU Hui, GE Bin-cheng, XIN Yun-chang, WU Rui-zhi, FERNANDEZ C, HUANG Jian-yu, PENG Qiu-ming. Achieving high strength and ductility in magnesium alloys via densely hierarchical double contraction nanotwins [J]. Nano Letters, 2017, 17(10): 6117−6124.

[12] LENTZ M, RISSE M, SCHAEFER N, REIMERS W, BEYERLEIN I J. Strength and ductility with $\{10\bar{1}1\}-\{10\bar{1}2\}$ double twinning in a magnesium alloy [J]. Nature Communications, 2016, 7(1): 11068.

[13] BROWN D W, AGNEW S R, BOURKE M A M, HOLDEN T M, VOGEL S C, TOMÉ C N. Internal strain and texture evolution during deformation twinning in magnesium [J]. Materials Science and Engineering A, 2005, 399(1): 1−12.

[14] KNEZEVIC M, LEVINSON A, HARRIS R, MISHRA R K, DOHERTY R D, KALIDINDI S R. Deformation twinning in AZ31: Influence on strain hardening and texture evolution [J]. Acta Materialia, 2010, 58(19): 6230−6242.

[15] YIN S M, YANG F, YANG X M, WU S D, LI S X, LI G Y. The role of twinning−detwinning on fatigue fracture morphology of Mg−3%Al−1%Zn alloy [J]. Materials Science and Engineering A, 2008, 494(1): 397−400.

[16] PRASAD N S, KUMAR N N, NARASIMHAN R, SUWAS S. Fracture behavior of magnesium alloys−Role of tensile twinning [J]. Acta Materialia, 2015, 94: 281−293.

[17] REED-HILL R E, ROBERTSON W D. Additional modes of deformation twinning in magnesium [J]. Acta Materialia, 1957, 5(12): 717−727.

[18] KOIKE J. Enhanced deformation mechanisms by anisotropic plasticity in polycrystalline Mg alloys at room temperature [J]. Metallurgical and Materials Transactions A, 2005, 36(7): 1689−1696.

[19] BEYERLEIN I J, CAPOLUNGO L, MARSHALL P E, MCCABE R J, TOMÉ C N. Statistical analyses of deformation twinning in magnesium [J]. Philosophical Magazine, 2010, 90(16): 2161−2190.

[20] KUMAR M A, BEYERLEIN I J. Local microstructure and micromechanical stress evolution during deformation twinning in hexagonal polycrystals [J]. Journal of Materials Research, 2020, 35(3): 217−241.

[21] KUMAR M A, WROŃSKI M, MCCABE R J, CAPOLUNGO L, WIERZBANOWSKI K, TOMÉ C N. Role of microstructure on twin nucleation and growth in HCP titanium: A statistical study [J]. Acta Materialia, 2018, 148: 123−132.

[22] SHI Z Z, ZHANG Y, WAGNER F, JUAN P A, BERBENNI S, CAPOLUNGO L, LECOMTE J S, RICHETON T. On the selection of extension twin variants with low Schmid factors in a deformed Mg alloy [J]. Acta Materialia, 2015, 83: 17−28.

[23] CHAI Yan-qin, BOEHLERT C J, WAN You-fu, HUANG Guang-hao, ZHOU Hao, ZHENG Jiang, WANG Qu-dong, YIN Dong-di. Anomalous tension twinning activity in extruded Mg sheet during hard-orientation loading at room temperature [J]. Metallurgical and Materials Transactions A, 2021, 52(2): 449−456.

[24] WANG F, SANDLÖBES S, DIEHL M, SHARMA L, ROTERS F, RAABE D. In situ observation of collective grain-scale mechanics in Mg and Mg-rare earth alloys [J]. Acta Materialia, 2014, 80: 77−93.

[25] TAHREEN N, CHEN D L, NOURI M, LI D Y. Influence of aluminum content on twinning and texture development of cast Mg−Al−Zn alloy during compression [J]. Journal of Alloys and Compounds, 2015, 623: 15−23.

[26] HAN J, SU X M, JIN Z H, ZHU Y T. Basal-plane stacking-fault energies of Mg: A first-principles study of Li- and Al-alloying effects [J]. Scripta Materialia, 2011, 64(8): 693−696.

[27] HUANG Guang-hao, YIN Dong-di, LU Jia-wei, ZHOU Hao, ZENG Ying, QUAN Gao-feng, WANG Qu-dong. Microstructure, texture and mechanical properties evolution of extruded fine-grained Mg−Y sheets during annealing [J]. Materials Science and Engineering A, 2018, 720: 24−35.

[28] LONG Li-jun, HUANG Guang-hao, YIN Dong-di, JI Bin, ZHOU Hao, WANG Qu-dong. Effects of Y on the deformation mechanisms of extruded Mg−Y sheets during room-temperature compression [J]. Metallurgical and Materials Transactions A, 2020, 51: 2738−2751.

[29] YIN Dong-di, BOEHLERT C J, LONG Li-jun, HUANG Guang-hao, ZHOU Hao, ZHENG Jiang, WANG Qu-dong. Tension-compression asymmetry and the underlying slip/twinning activity in extruded Mg−Y sheets [J]. International Journal of Plasticity, 2021, 136: 102878.

[30] JAHEDI M, MCWILLIAMS B A, MOY P, KNEZEVIC M. Deformation twinning in rolled WE43-T5 rare earth magnesium alloy: Influence on strain hardening and texture evolution [J]. Acta Materialia, 2017, 131: 221−232.

[31] HIELSCHER R, SILBERMANN C, SCHMIDL E, IHLEMANN J. Denoising of crystal orientation maps [J]. Journal of Applied Crystallography, 2019, 52: 984−996.

[32] BACHMANN F, HIELSCHER R, SCHAEBEN H. Texture analysis with MTEX-free and open source software toolbox [J]. Solid State Phenomena, 2010, 160: 63−68.

[33] LU Jia-wei, YIN Dong-di, REN Ling-bao, QUAN Gao-feng. Tensile and compressive deformation behavior of peak-aged cast Mg−11Y−5Gd−2Zn−0.5Zr (wt.%) alloy at elevated temperatures [J]. Journal of Materials Science, 2016, 51(23): 10464−10477.
[34] NI Ran, MA Shi-jun, LONG Li-jun, ZHENG Jiang, ZHOU Hao, WANG Qu-dong, YIN Dong-di. Effects of precipitate on the slip activity and plastic heterogeneity of Mg−11Y−5Gd−2Zn−0.5Zr (wt.%) during room temperature compression [J]. Materials Science and Engineering A, 2021, 804: 140738.
[35] CHAPUIS A, DRIVER J H. Temperature dependency of slip and twinning in plane strain compressed magnesium single crystals [J]. Acta Materialia, 2011, 59(5): 1986−1994.
[36] KOCKS U F, TOMÉ C N, WENK H. Texture and anisotropy [M]. Cambridge University Press, 1998.
[37] KULA A, JIA Xiao-hui, MISHRA R K, NIEWCZAS M. Mechanical properties of Mg−Gd and Mg−Y solid solutions [J]. Metallurgical and Materials Transactions B, 2016, 47(6): 3333−3342.
[38] CEPEDA-JIMÉNEZ C M, PÉREZ-PRADO M T. Microplasticity-based rationalization of the room temperature yield asymmetry in conventional polycrystalline Mg alloys [J]. Acta Materialia, 2016, 108: 304−316.
[39] JIANG L, JONAS J J, LUO A A, SACHDEV A K, GODET S. Influence of $\{10\bar{1}2\}$ extension twinning on the flow behavior of AZ31 Mg alloy [J]. Materials Science and Engineering A, 2007, 445/446: 302−309.
[40] MARSHALL P E, PROUST G, ROGERS J T, MCCABE R J. Automatic twin statistics from electron backscattered diffraction data [J]. Journal of Microscopy, 2010, 238(3): 218−229.
[41] KOIKE J, SATO Y, ANDO D. Origin of the Anomalous $\{10\bar{1}2\}$ twinning during tensile deformation of Mg alloy sheet [J]. Materials Transactions, 2008, 49(12): 2792−2800.
[42] GITHENS A, GANESAN S, CHEN Z, ALLISON J, SUNDARARAGHAVAN V, DALY S. Characterizing microscale deformation mechanisms and macroscopic tensile properties of a high strength magnesium rare-earth alloy: A combined experimental and crystal plasticity approach. [J]. Acta Materialia, 2020, 186: 77−94.
[43] ABUZAID W Z, SANGID M D, CARROLL J D, SEHITOGLU H, LAMBROS J. Slip transfer and plastic strain accumulation across grain boundaries in Hastelloy X [J]. Journal of the Mechanics and Physics of Solids, 2012, 60(6): 1201−1220.
[44] DELLA VENTURA N M, KALÁCSKA S, CASARI D, EDWARDS T E J, SHARMA A, MICHLER J, LOGÉ R, MAEDER X. $\{10\bar{1}2\}$ twinning mechanism during in situ micro-tensile loading of pure Mg: Role of basal slip and twin-twin interactions [J]. Materials & Design, 2021, 197: 109206.
[45] JEONG J, ALFREIDER M, KONETSCHNIK R, KIENER D, OH S H. In-situ TEM observation of $\{10\bar{1}2\}$ twin-dominated deformation of Mg pillars: Twinning mechanism, size effects and rate dependency [J]. Acta Materialia, 2018, 158: 407−421.
[46] HU Y, TURLO V, BEYERLEIN I J, MAHAJAN S, LAVERNIA E J, SCHOENUNG J M, RUPERT T J. Embracing the chaos: alloying adds stochasticity to twin embryo growth [J]. Physical Review Letters, 2020, 125(20): 205503.
[47] STANFORD N, MARCEAU R K W, BARNETT M R. The effect of high yttrium solute concentration on the twinning behaviour of magnesium alloys [J]. Acta Materialia, 2015, 82: 447−456.
[48] HE Cong, LI Zhi-qiao, KONG De-hao, ZHAO Xiao-jun, CHEN Hou-wen, NIE Jian-feng. Origin of profuse $\{11\bar{2}1\}$ deformation twins in Mg−Gd alloys [J]. Scripta Materialia, 2021, 191: 62−66.

钇含量在挤压 Mg−Y 板材拉伸/压缩变形下孪生行为中的作用

柴艳琴[1]，尹冬弟[1]，华 珅[1]，黄广号[1]，周 浩[2]，郑 江[3]，王渠东[4]

1. 西南交通大学 材料科学与工程学院 材料先进技术教育部重点实验室，成都 610031；
2. 南京理工大学 材料科学与工程学院 纳米异构材料中心，南京 210094；
3. 重庆大学 材料科学与工程学院 教育部轻合金材料国际合作联合实验室 沈阳材料科学国家研究中心，重庆 400044；
4. 上海交通大学 材料科学与工程学院 轻合金精密成型国家工程研究中心，上海 200240

摘 要：研究 Y 含量对挤压 Mg−xY (x=0.5, 1, 1.5，质量分数，%)板材在沿挤压方向单轴拉伸和压缩下的晶粒尺度孪生行为的影响。基于电子背散射衍射(EBSD)，获得大量数据(包括 2691 个晶粒和 977 个孪晶)，并对其运用自动孪晶变体分析方法。结果表明，无论拉伸还是压缩，都是 $\{10\bar{1}2\}$ 拉伸孪晶(TTW)主导变形，并出现大量反常孪生行为(施密特因子(m)<0)。反常孪生行为在拉伸下随着 Y 含量增加更加明显，表明更高含量的 Mg−Y 合金中孪生变体选择更加随机。然而，在压缩下依赖于 Y 含量的反常孪生行为是相反的。研究还发现，反常拉伸孪晶的比例在拉伸和压缩下分别与相应母晶粒中基面和柱面滑移的最大施密特因子(m_{max})密切相关，表明当前 Mg−Y 合金中孪生和滑移或许有着密切联系。

关键词：镁稀土合金；变形孪生；孪晶变体选择；施密特因子；反常孪晶

(Edited by Bing YANG)